Available online at www.sciencedirect.com
ScienceDirect
Ceramics International 34 (2008) 2017–2024
CERAMICS INTERNATIONAL
www.elsevier.com/locate/ceramint

Thermal shock behavior of dense mullite–zirconia composites obtained by two processing routes

Nicolás M. Rendtorff, Liliana B. Garrido, Esteban F. Aglietti *

Centro de Tecnología de Recursos Minerales y Cerámica (CETMIC: CIC-CONICET-UNLP), Camino Centenario y 506, C.C. 49 (B1897ZCA) M.B. Gonnet, Buenos Aires, Argentina

Received 11 January 2007; received in revised form 16 May 2007; accepted 24 July 2007
Available online 24 August 2007

Abstract

Mullite–zirconia composites were prepared using two different processing routes such as reaction sintering (RS) of alumina and zircon and direct sintering of mullite–zirconia grains. For the RS process, alumina and zircon (AZ) as raw materials were used, while in the other route mullite–zirconia-electrofused grains (MZ) previously mixed with a second ceramic phase as a binder were employed. These both types of ceramics were produced by slip casting in plaster molds and finally sintered at 1600 °C for 2 h. In this work, the microstructure and the resistance to thermal shock for both high-density mullite–zirconia composites were studied. For materials characterization, density, XRD and SEM techniques were employed. Thermal shock behavior was determined by quenching in water with ΔT of 200–1200 °C and for 1–10 repeated cycles for each ΔT used. The variation of damage with thermal shock severity was followed by measuring the dynamic elastic modulus E using the impulse excitation method.

The two processing routes resulted in ceramic composites with similar phase contents, but with microstructural differences. The dependence of elastic modulus on severity of thermal shock was in accordance with literature predictions, where below a critical quenching temperature difference (ΔT_c) no degradation in the elastic behavior was found.

The thermal shock resistance increased when zircon was used as bonding phase, rather than alumina or alumina–zircon mix.

Keywords: Mullite–zirconia; Ceramic processing; Thermal shock; Elastic modulus

1. Introduction

Mullite–zirconia composites are materials with important technological applications due to their good properties such as toughness, chemical stability, and high-creep resistance. In practice they are employed in the glass industry and where a high chemical and corrosion stabilities are required. Zircon and alumina are largely employed as raw materials in their manufacture [1–6]. Composites with zirconia and mullite as the main phases can be also produced from some of the commercial types of grains MZ coming from an electrofusion process. This processing route involves the utilization of finely ground MZ powder with a bonding phase (alumina, zircon, etc.) because single electrofused grains are not easy to be sintered.

Although, mullite and zirconia are the major constituents in the composite, the physical characteristics, microstructure and properties of the resulting ceramic may be different [1–11].

The first approach to determine the thermal stresses of brittle material is a thermoelastic theory [12], which is focused in the initiation of the fracture. A second approach focuses on crack propagation for conditions of thermal shock more severe than those for crack initiation [13].

A unified theory of the thermal shock resistance considering the initiation and crack propagation in brittle ceramics is due to Hasselman [14] who presented analytical solutions for the extent of the cracks as a function of the severity of the thermal shock.

The thermal shock resistance is improved by the deliberate introduction of thermal stress concentrators in the form of microstructural inhomogeneities in the material. Thus, the dispersion of zirconia grains in a mullite matrix, improves the thermomechanical behavior as a result of microcracks formation and by the dissipation of elastic energy related to zirconia martensitic transformation [15].

* Corresponding author. Tel.: +54 2214840247; fax: +54 2214710075.
E-mail address: eaglietti@cetmic.unlp.edu.ar (E.F. Aglietti).

0272-8842/$34.00
doi:10.1016/j.ceramint.2007.07.035

There is not known a simple and universal test to evaluate the behavior of ceramic materials to thermal shock (TS) and also capable to be extrapolated to the actual conditions in service, sample geometry, and thermal cycles. However, some experimental tests consisting in sudden heating and cooling are easy to made but they have only a comparative value between similar materials. Practical tests for evaluating the thermal shock resistance determine the variation or change of some characteristic property of the test sample. The TS can be evaluated on heating or cooling, but in most methods a sudden cooling step is used because its greater severity. A method consists in heating the test probe to a desirable temperature; followed by rapid cooling to room temperature (referred to us the quenching method), by immersion in liquids such as water, oil or alcohol, etc. [16]. A characteristic mechanical property like fracture strength or elastic modulus is measured before and after quenching. In this way the severity of the treatment can be studied by determining the relative drop in mechanical strength or elastic modulus after exposure at a given thermal cycle. Also the damage in the material can be correlated after application of repeated thermal cycles.

2. Experimental

Conventional methods to evaluate the elastic modulus E are complicated and destructive. An alternative method is the dynamic E modulus determination using the impulse excitation (sonic velocity) that is a simple and non-destructive standard test [17].

In this work, the microstructure and thermal shock behavior of mullite–zirconia ceramics were studied. Two types of composites were obtained through different processing routes: one of them using RS method and the other by sintering a commercial mullite–zirconia powder using a bonding phase as a sintering aid. Both materials were formed by slip casting in plaster molds. The probes were prismatic bars because the determination of the E modulus is easier and more reproducible employing this geometry. The sintered composites (1600 °C–2 h) were characterized in terms of microstructure and physical properties. The influence of the addition of different bonding phases was also analyzed.

2.1. Preparation of mullite–zirconia composites by reaction sintering

The mullite–zirconia composite AZ was prepared using a stoichiometric mixture of alumina and zircon. Starting powders were commercially available: alumina (α-Al_2O_3, A-16SG, Alcoa Inc., USA) and zircon ($ZrSiO_4$, Mahlwerke Kreutz, Mikron, Germany) with unimodal narrow particle size distributions (average particle sizes: 0.6 and 1.8 μm; specific surface areas BET: 9.5 and 4.1 m^2/g, respectively).

The alumina–zircon powder mixture was prepared with an alumina to zircon weight ratio of 45.5:54.5 (wt.%), respectively. Stabilized 48 vol.% aqueous suspension was obtained using 0.24 wt.% of Dolapix CE64 (Zschimmer and Schwartz) as a dispersant at pH 9.1. Previous studies with this mixture indicated that compacts prepared from suspension in this condition had low-total volume of small pores [4,5]. Therefore bars were produced from the optimal slip condition of the mixture by slip casting in a plaster mold, dried at room temperature and then at 110 °C. Finally the prismatic 8 mm × 8 mm × 50 mm bars were sintered at 1600 °C–2 h.

Table 1
Typical chemical analysis of the MZVR from ELFUSA (www.elfusa.com.br)

Oxide	wt.%
Al_2O_3	44.02
TiO_2	0.29
SiO_2	17.96
Fe_2O_3	0.11
MgO	0.09
CaO	0.18
Na_2O	0.16
K_2O	0.04
ZrO_2	39.13

2.2. Preparation of mullite–zirconia composites from an electrofused MZ powder

A commercial mullite–zirconia grains was employed as starting powder. This material (MVZR, Elfusa Ltd., Brasil) is produced from pure raw materials by an electrofusion process in electric arc furnaces. The chemical analysis is shown in Table 1. Additional information provided by the manufacturer: melting point 1850 °C, apparent density 3.71 g/cm^3; apparent porosity 3.0%; true density 3.74 g/cm^3; reversible thermal expansion at 1400 °C 0.68%.

A size fraction with mean particle diameter (d_{50}) lower than 10 μm (obtained by a sedimentation process) was attrition milled to reduce d_{50} to 5 μm. This fine powder contains mullite and monoclinic zirconia (m-ZrO_2) as crystalline phases and was used as starting material (MZ).

As bonding phases were used: α-alumina (α-Al_2O_3 d_{50} = 0.45 μm, A-16SG, Alcoa Inc., USA) and zircon ($ZrSiO_4$ d_{50} = 2 μm Mahlwerke Kreutz, Mikron, Germany).

The mixtures of MZ and the bonding additives were prepared with a proportion of 85 wt.% of MZ and 15 wt.% of sintering aids. Three compositions were prepared: (a) with α-alumina (MZa), (b) with zircon (MZz) and (c) employing as a bonding phase an stoichiometric mixture of α-Al_2O_3 and zircon (45.5/54.5 wt.%) (MZaz).

The prismatic bars 7.5 mm × 7.5 mm × 50 mm were produced from well-dispersed suspensions by slip casting in a plaster molds as previously described [5].

2.3. Characterization methods

Crystalline phases formed by sintering were analyzed with DRX equipment (Philips 3020 with Cu Kα radiation in Ni filter at 40 kV–20 mA). The relative content of tetragonal ZrO_2 was determined using the Garvie and Nicholson method [18] which is based on the integrated peak areas of the phases of zirconia present.

The dilatometry of the sintered probes was made up to 1350 °C with a heating rate of 10 °C/min in a Netzsch Inc. equipment.

Microstructure of polished samples was observed with a scanning electron microscope SEM (JEOL JSM 6360 LV).

The dynamic elastic modulus E of the sintered bars was measured by the impulse excitation technique (Grindosonic, MK5 model).

Thermal shock tests were performed using a quenching method employing cycles with quenching temperature differentials ΔT of 200, 400, 600, 800, 1000 and 1200 °C. The probes were initially heated in an electric furnace for 90 min and then suddenly cooled in water at 25 °C. The damage produced by the severity of the thermal shock test was evaluated by measurements of the E modulus for 1–10 repeated quenching cycles at a given ΔT.

The theoretical E modulus of the materials was calculated using the Voight model with the volume fraction of each constituent in accordance with the composition determined by DRX (Table 3), using values of Young modulus at zero porosity E_0: mullite 210 GPa, m-ZrO_2 200 GPa, alumina 380 GPa, zircon 190 GPa and fused silica 70 GPa [19,20].

3. Results and discussion

In Table 2 the physical characteristics of the materials sintered at 1600 °C–2 h are shown. The sintered AZ samples and those prepared from MZ mixtures with different bonding phases, achieved similar final densities and low porosity (lower than 5%). Also, the probes exhibited low-water absorption.

The diffractograms of MZ mixtures sintered at 1600 °C–2 h (Fig. 1) showed mullite and m-ZrO_2 as the principal crystalline phases. Tetragonal zirconia (t-ZrO_2) also appeared after sintering. This phase was not present in the starting powder MZ. Using the Garvie and Nicholson method [18] the relative t-ZrO_2 content was estimated near 4% of the total zirconia.

The AZ sample was also mainly composed by mullite and m-ZrO_2 but low-intensity peaks of alumina and zircon were detected evidencing that reaction-sintering was not completed.

The MZa sample had a low content of residual alumina as shown in Fig. 1. The non-reacted alumina can be observed as dark areas in the SEM micrograph (Fig. 3). For the MZz sample, zircon disappeared as a minor phase, indicating that its thermal decomposition was complete. Zircon dissociation produces zirconia and silica and generally takes place at temperatures near to 1600 °C, but in the presence of alumina, decomposition occurs at a relatively low temperature (near

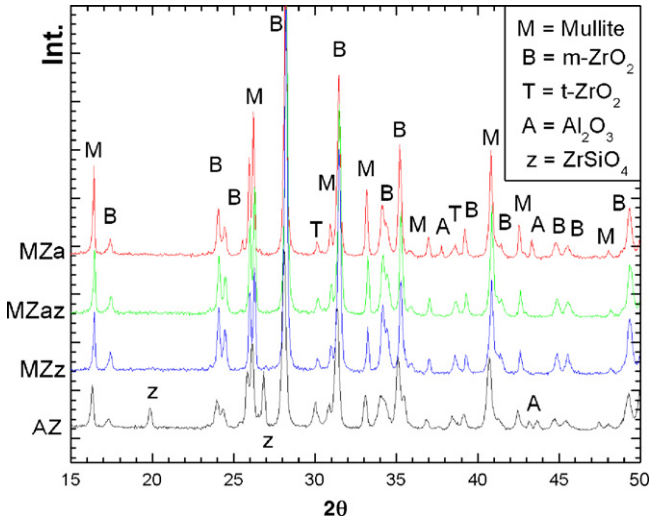

Fig. 1. XRD patterns of the different composites studied.

1450 °C). Zirconia remained as a monoclinic form whereas silica probably generated a glassy phase or resulted in a formation of mullite as a solid solution with excess of silica.

Table 2 shows the experimental and calculated E values of the sintered samples for the different compositions. The theoretical E value of composites was calculated considering the volume fraction (Table 3) and E_0 of each constituent.

The experimental value of E of the AZ composite was approximately 90% of the theoretical value obtained using the Voight model and taken into account the volume fraction of each phase. However, for MZ materials only the experimental E value of the MZaz specimen reached around 80% of the calculated. The measured E values for MZa and MZz were 70–75% of the calculated ones.

The experimental E values were lower than the calculated ones. Residual porosity and processing defects are probably responsible for this fact. The E value of AZ materials was higher than those determined for MZ compositions; this was probably due to the different phase composition and final microstructure. Generally zircon addition caused a reduction of E and as expected, experimental values of E increased with increasing the alumina content.

For the MZa composition, the intensity of alumina DRX peaks decreased after sintering which means that it formed mullite solid solution or remained as crystalline phase, however it is not well evidenced by DRX.

The diffractograms of MZz indicated that thermal decomposition of zircon was completed, as no peaks of this phase was

Table 2
Properties and theoretical and experimental elastic modulus E_0 for the different mullite–zirconia composites sintered at 1600 °C

Material	Green density (g/cm^3)	Bulk density (g/cm^3)	Apparent porosity (%)	Water absorption (%)	E_0 experimental (GPa)	E_0 calculated (GPa)
MZa	2.5	3.5	4.2	1.2	151	237
MZaz	2.4	3.6	2.9	0.7	162	204
MZz	2.3	3.6	3.2	0.9	139	193
AZ	2.6	3.7	<1.5	<0.5	189	219

AZ: reaction sintered, MZ: produced from milled MZ grains.

Table 3
Phase content of the different materials (in accordance with XRD diagrams)

Composite	Mullite (vol.%)	Total ZrO_2 (vol.%)	Alumina (vol.%)	Zircon (vol.%)	Silica (vol.%)
AZ	64.0	23.0	9.0	4.0	
MZa	62.8	22.5	≤14.7		
MZaz	74.0	26.0			
MZz	63.3	29.3			≤7.4

observed whereas additional zirconia appeared and silica formation probably resulted in a development of glassy phase or in mullite solid solution.

For MZaz sample the reaction between alumina and zircon was completed resulting in some zirconia and mullite formation.

3.1. Microstructure

The characteristics of the materials obtained by the two processing routes were similar when the principal crystalline phases are considered, but there existed differences in the microstructures that possibly caused the different TS behavior.

Figs. 2–5 show that both composites had a dense microstructure with low-residual pore presence. Two types of grains were noticeable: dispersed grains (white) of zirconia, and a mullite matrix (gray).

Fig. 2 shows the AZ microstructure with a mullite dense matrix in which the development of grain boundaries was clearly visible. Inter and intragranular ZrO_2 grains (white) were observed. Zirconia intergranular grains also appeared as agglomerates with pores located between them. Intragranular ZrO_2 grains were finer (<1 μm) with a spherical shape. Previous studies [21] using special XRD techniques revealed that intragranular particles are tetragonal ZrO_2, while much of the intergranular ZrO_2 is monoclinic. Intergranular zirconia grains increased up to 2–3 μm and exhibited a rounded shape. Some of mullite grains showed a change in shape from rounded to slightly elongated.

Microstructures of MZa MZaz and MZz are shown in Figs. 3–5, respectively. In these materials intergranular m-ZrO_2 and mullite were also observed, but intragranular t-ZrO_2 was not present. In these photographs the boundaries of mullite grains were clearly identified. For these samples ZrO_2 grain size ranged between 1 and 7 μm which were significantly larger than those of starting MZ grains. This fact indicates that the sintering conditions employed (1600 °C–2 h) was hard enough to reach sintering and therefore, the coalescence of isolated zirconia grains probably took place. Some zirconia grains appeared in contact forming a well-developed neck which therefore means that sintering can be made at lower

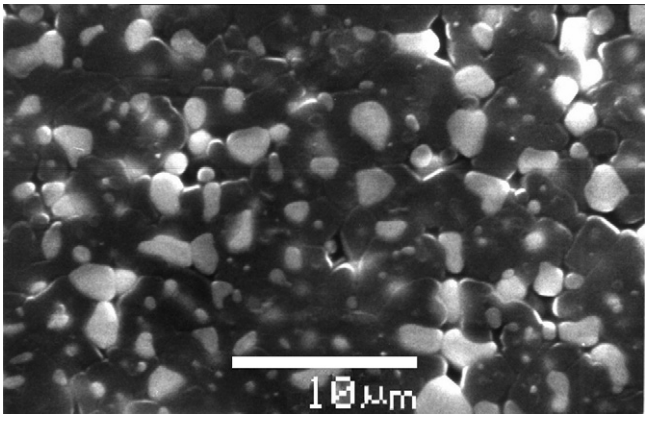

Fig. 2. SEM micrograph of the AZ specimen obtained by reaction sintering.

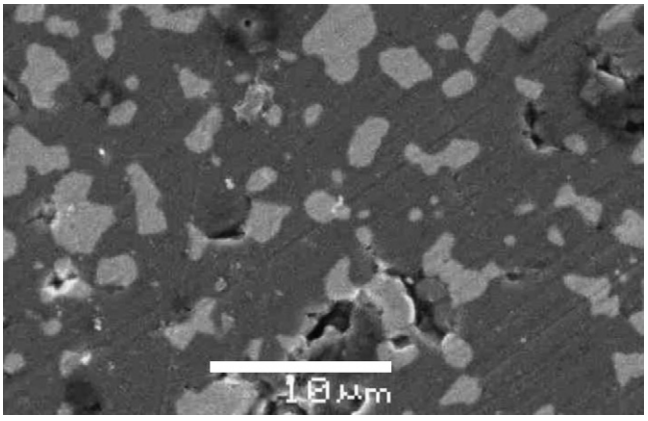

Fig. 3. SEM micrograph of the MZa specimen obtained from electrofused powders of mullite–zirconia with alumina as sintering phase.

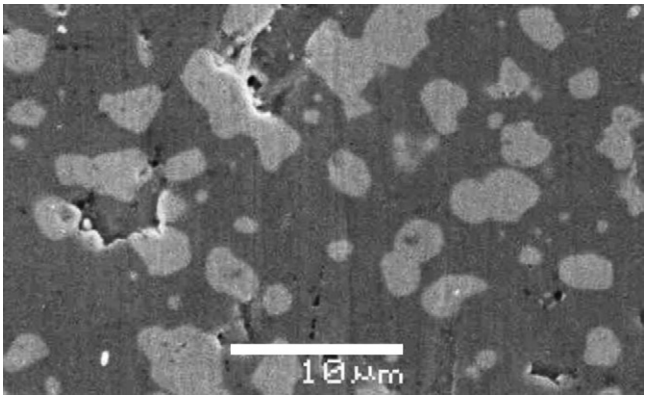

Fig. 4. SEM micrograph of the MZaz specimen obtained from electrofused powders of mullite–zirconia with a stoichiometric mixture of alumina and zircon as sintering phase.

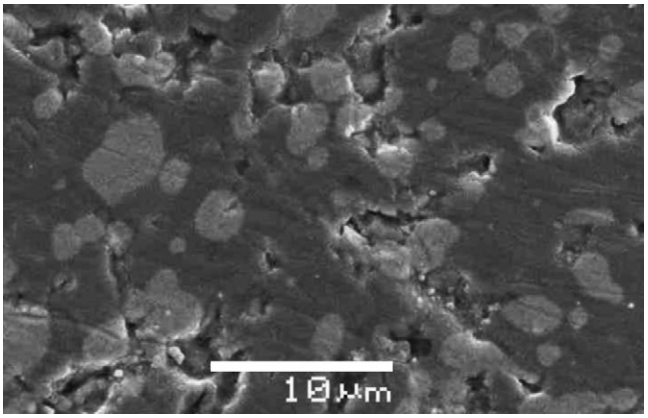

Fig. 5. SEM micrograph of the MZz specimen obtained from electrofused powders of mullite–zirconia with zircon as sintering phase.

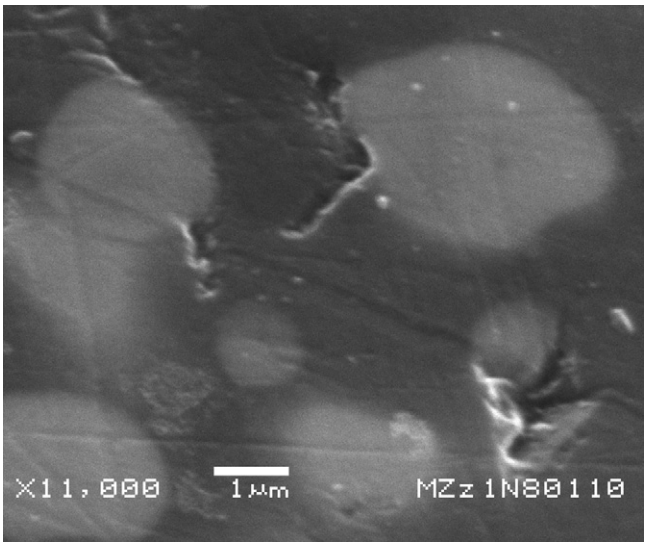

Fig. 6. SEM micrograph of the MZz specimen obtained from electrofused powders of mullite–zirconia with zircon as sintering phase showing microcracks in the mullite matrix.

temperatures. In MZa (Fig. 3) some dark grains corresponding to the remained alumina (reactant) were present. No t-ZrO_2 was observed using SEM, but DRX revealed the presence of this phase.

The AZ microstructure was characterized by rounded and isolated zirconia grains which tended to be comparatively smaller than that of MZ composites, whereas the mullite grain size are higher than that of MZ materials. AZ sample also exhibited the presence of t-ZrO_2 as intragranular small grains, with a size near to 1 μm.

Fig. 6 shows a detail of the MZz microstructure, where perpendicular to the zirconia-mullite grain boundary, microcracks in the mullite matrix can be seen as a consequence of the thermal expansion coefficient mismatch and the volume change associated with the ZrO_2 martensitic transformation during the cooling from the thermal treatment.

3.2. Dilatometry

The dilatometric curves of the RS and MZ composites are shown in Fig. 7. All of them presented a hysteresis loop area, due to the volume change associated to the m ↔ t transformation. This transformation begins at 1100 °C on heating and indicated that an important content of m-ZrO_2 was present. This transition occurred when the probes were sintered and when a thermal shock test for values of $\Delta T = 1000$ and 1200 °C. At 1600 °C the stable phase is the tetragonal form, but on cooling the monoclinic phase transformation took placed in those grains having a size higher than the critical one. In the same way for $\Delta T = 1200$ °C a complete transformation is expected, while a partial one will occur for $\Delta T = 1000$ °C.

The thermal expansion coefficient of all compositions was near 5.0×10^{-6} °C^{-1}, comparable with that of mullite (5.3×10^{-6} °C^{-1}) with no significant differences between materials.

3.3. Thermal shock behavior

3.3.1. Effect of the quenching temperature difference ΔT on E/E_0 ratio

Fig. 8 shows the variation of E/E_0 ratio (where E and E_0 are the measured elastic modulus before and after quenching, respectively) as a function of the quenching temperature difference ΔT for the RS and MZ composites after one thermal cycle. The E/E_0 ratio reduced with increasing ΔT and the E/E_0 drop was related to the damage induced in the materials mainly as changes in microstructure. The E/E_0 slightly reduced up to $\Delta T = 600$ °C, but for a range of ΔT between 600 and 1200 °C a pronounced and proportional reduction with ΔT was observed. The reduction in E was near 20% of the initial value for each 200 °C of ΔT applied.

The decrease in the elastic modulus can be attributed to the formation of cracks for ΔT greater than ΔT_c required for the initiation of crack formation.

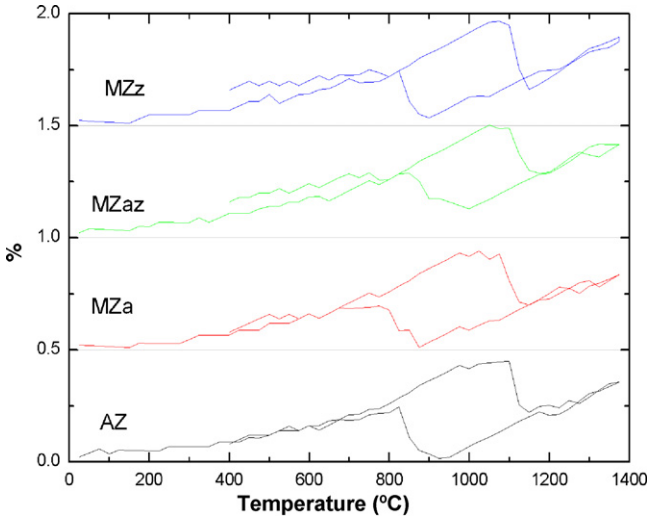

Fig. 7. Dilatometric and shrinkage curves of the different sintered composites as a function of the test temperature.

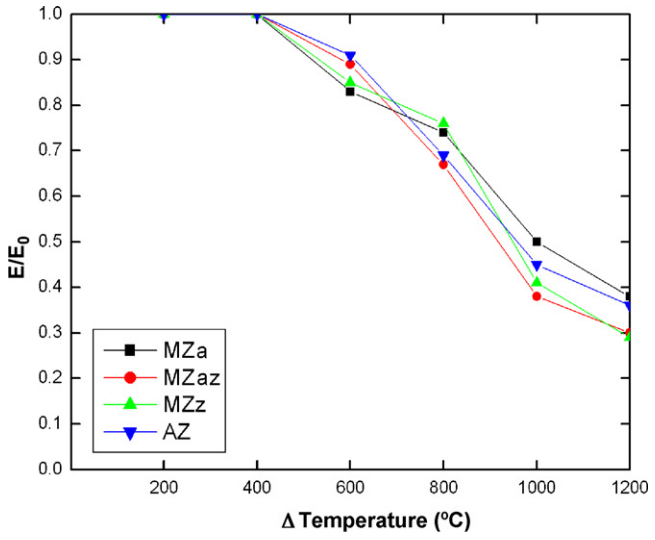

Fig. 8. Elastic modulus after and before one thermal cycle ratio (E/E_0) as a function of the quenching temperature difference ΔT.

The TS behavior of the materials studied is in accordance with predictions of Hasselman [14], when fracture strength versus ΔT is analyzed. The composites with thermal cycles below $\Delta T = 600\ ^\circ C$ did not suffer any damage because the elastic energies were less than the fracture energies required for the crack propagation. Above $\Delta T = 600\ ^\circ C$ a marked E reduction occurred indicating that the thermal stress induced the appearance of new microcracks or propagated those ones originally present.

Therefore the critical temperature ΔT_c of the materials was between 500 and 600 °C. The degree of the degradation induced by quenching from temperatures higher than ΔT_c depends on the size and toughness of the ceramic. Defects and microcracks are inherent in these materials because of their composition and processing methods chosen.

Above a critical value of crack length, microcracks can propagate in stable or unstable regime. In our materials the E behavior indicated that probably a stable crack propagation took place.

The critical length from which the cracks will propagate in a catastrophic way is near 0.1 mm [9] considering the dimensions of the probes employed. The surface defects observed in all probes (Figs. 2–5) were not higher than 5 μm (less than 10% of the critical size). In the original MZz microstructure (without thermal shock), microcracks in the mullite matrix were clearly visible which formed perpendicular to the zirconia grains. These microcracks came probably from the phase transformation on cooling from sintering temperature of zirconia grains that reached the critical size for t → m transformation. Therefore, a decrease in E/E_0 may be explained by the extent of the microcraks, but these phenomena did not occur in a catastrophic way. When thermal shocks applied was $\Delta T = 1200\ ^\circ C$ a 70% reduction in E/E_0 was observed, and many probes failed during the quenching (i.e. the microcracks propagated in a catastrophic way). Thus, in order to observe the effect of the number of applied cycles ΔT of 1000, 800, and 600 °C were employed.

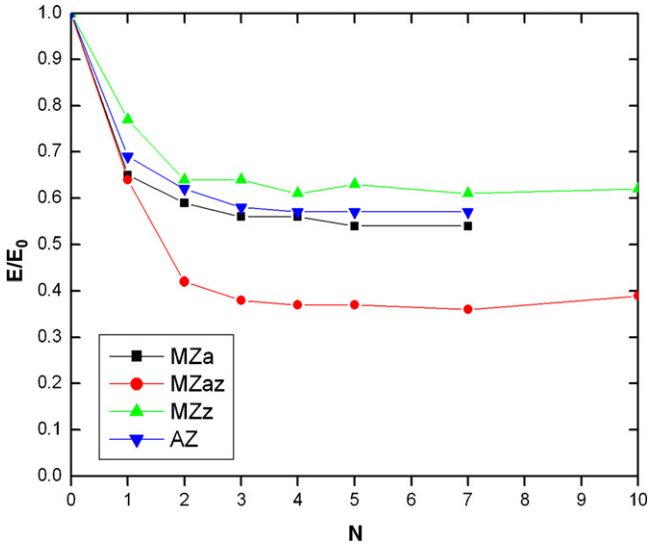

Fig. 10. Elastic modulus after and before thermal cycles ratio (E/E_0) as a function of the number of cycles of $\Delta T = 800\ ^\circ C$.

3.3.2. *Effect of repeated thermal shock cycles on E/E_0*

Fig. 9 shows the effect of the number of thermal shock cycles at $\Delta T = 600\ ^\circ C$ on the E/E_0 for the different composites. The E/E_0 strongly reduced for two cycles and then remained nearly constant (85–90%). The AZ probes showed a relatively high-E/E_0 ratio than that of the other materials. The E reduction after the first thermal cycle indicated that development of microcracks was sufficient to avoid the propagation and to increase the thermal shock resistance to further thermal cycles. The microcrack formation after the first cycle avoided crack propagation and growth. Microcracking as stress dissipation mechanism was generated by thermal shock.

Fig. 10 shows that after the first thermal cycle of $\Delta T = 800\ ^\circ C$ a reduction in E close to 25–30% of the E_0 was observed for AZ, MZa, MZaz and MZz probes. For the second and third cycles the E/E_0 reduced to 40% for AZ, MZa,

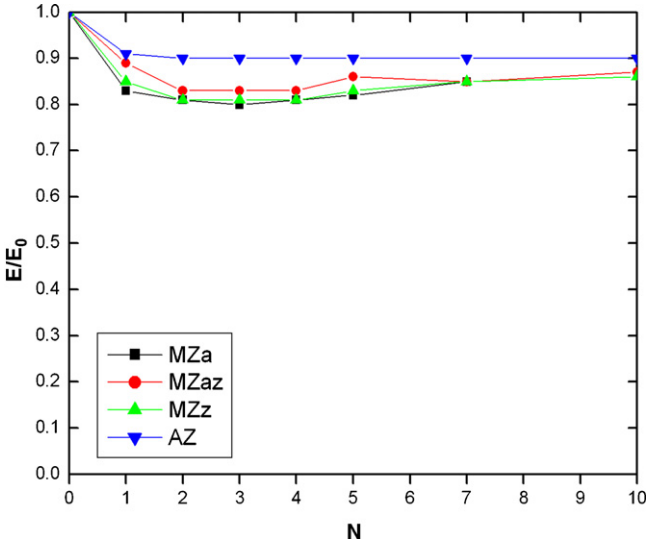

Fig. 9. Elastic modulus after and before thermal cycles ratio (E/E_0) as a function of the number of cycles of $\Delta T = 600\ ^\circ C$.

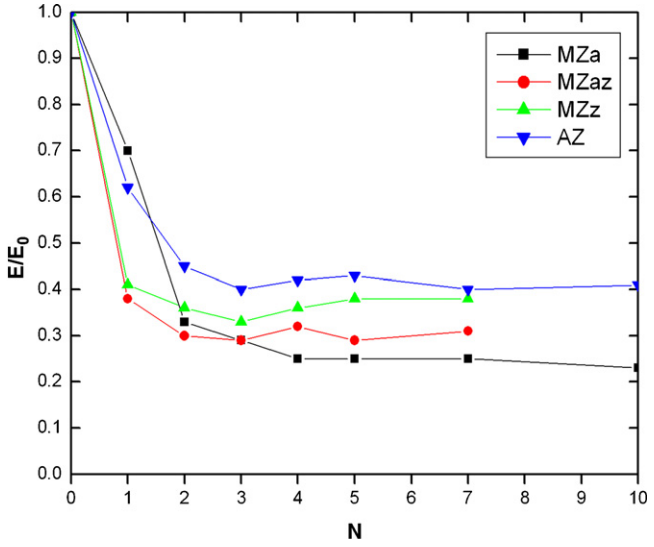

Fig. 11. Elastic modulus after and before thermal cycles ratio (E/E_0) as a function of the number of cycles of $\Delta T = 1000\ ^\circ C$.

and MZz. For MZaz after 10 cycles the E reduction was 60% of the original value.

The thermal shock with $\Delta T = 1000\ ^\circ C$ (Fig. 11), produced after one cycle an E drop of 30% of E_0 in probes AZ and MZa, but for MZz and MZaz the decrease in E was comparatively more important (near 60%). For AZ composites E retained near 45% of its original value after several cycles. However, the probes elaborated with MZ grains showed that E was only 30% of the original one.

The appearance of microcracks due to $t \leftrightarrow m$ ZrO_2 transformation (under cooling) increases with ZrO_2 content. In MZz sample ZrO_2 content was slightly higher than that of others, because of additional zirconia resulting from zircon dissociation (Table 3). Therefore, the better behavior of MZz and MZaz with respect to MZa composition may be explained by a relatively high density of microcracks which damped the effects of the successive cycles. In these experiences only a 30% of the probes failed after subjected to $\Delta T = 1000\ ^\circ C$ during 10 cycles.

The very large drop in E/E_0 for MZaz with increasing the number of cycles was probably related to the presence of alumina (the phase with high E) that increased the stiffness of the matrix.

3.3.3. Effect of the powder composition on the thermal shock behavior

In brittle materials the fracture mechanism starts from a unique defect and when it reaches the critical size the propagation of the cracks occurs in a catastrophic way. The real problem is the largest defect and the microstructure parameters are closely related to it. Microstructural factors are related to processing conditions and include: size, number and distribution of microcracks, grains and pores. In zirconia containing materials martensitic transformation is also an important factor. Zirconia has a thermal expansion coefficient ($10.0 \times 10^{-6}\ ^\circ C^{-1}$) twice of mullite ($5.3 \times 10^{-6}\ ^\circ C^{-1}$). Consequently, the expansion thermal mismatch between grains and matrix in the composites caused a considerable interface stress and microcracks resulting in decrease in the elastic modulus.

The effect of different powder compositions was observed using tests with $\Delta T = 800$ and $1000\ ^\circ C$. For both cases the best results were obtained when zircon (15 wt.%) was added as sintering agent showing retention of 40% of the original E value.

For MZ series, zircon was the best additive for thermal shock resistance for $\Delta T = 800$ and $1000\ ^\circ C$. Thermal decomposition of zircon increased the zirconia content. The formation of microcracks with a size below the critical one is preferred, as they can act as sink of stress and energy. Thereby increasing the TS resistance after one or more successive cycles. In consequence, the additions of zirconia (in adequate percentages) to a mullite matrix improved the thermal shock resistance due to the formation of the great amount of microcracks. Similar effect is caused by microporosity [22].

The behavior of MZaz was different, at $\Delta T = 800\ ^\circ C$ the reduction of E/E_0 with successive cycles was a 20% higher than the MZ samples. But at $\Delta T = 1000\ ^\circ C$ the observed suffered damage was greater than that of MZz, but lower than the observed for MZa. These results suggested a direct relation between the zirconia content (i.e. the presence of microcracks) and the thermal shock behavior. The thermal cycle at $1000\ ^\circ C$ induced the microcrack formation due to $t \leftrightarrow m$ transformation; this effect did not take place at $800\ ^\circ C$.

The AZ composites showed the best behavior to thermal shock test which may result from the microstructural characteristics achieved using the RS process. The resulting microstructure possessed optimal features such as a comparatively low-grain size of the intergranular zirconia (1–2 μm) and a (narrow) uniform distribution of the fine intragranular zirconia (<1 μm). These characteristics in combination with the appearance of microcracks whose size was below the critical length were favorable to enhancing the thermal shock resistance. Also, crack propagation was prevented possibly by the matrix compression due to the amount of transformable tetragonal phase. Additionally, the presence of anisotropic (elongated) mullite crystals can also deflect crack path propagation.

4. Conclusions

The impulse excitation technique was an useful method to evaluate the elastic modulus and therefore, was used to detect the microstructural damage of mullite–zirconia ceramics after exposure to thermal shock test. The thermal shock resistance of composites obtained through two different processing techniques (RS and sintering of mullite–zirconia grains) was analyzed. In both cases the forming method was slip casting in plaster molds.

The thermal shock test produced a decrease in the elastic modulus with increasing the applied ΔT. Internal microcracks were generated. The successive thermal cycles delayed in a well-defined behavior. After two thermal cycles, E remained nearly constant showing that the material had a great resistance to crack propagation and growth.

For $\Delta T = 1200\ ^\circ C$ an important damage was produced when the second cycle was performed, because the cracks reached a super-critical size.

The two processing routes conducted to similar phase composition but differences in microstructure were observed. These differences comprise: shape and size of intergranular zirconia, t-ZrO_2 content, and probably the mullite crystal morphology. The best performance of the AZ material may be explained by these factors.

Materials made from electrofused mullite–zirconia grains with the addition of alumina, zircon or a mixture of both, showed a similar behavior to thermal shock for ΔT of 200, 400, 600, and $1200\ ^\circ C$. But for ΔT 800 and $1000\ ^\circ C$ quite different behavior was observed because these values of ΔT were near to $t \leftrightarrow m$ transformation temperature.

The thermal shock resistance improved when zircon was used as bonding phase. The materials with alumina have a relatively good resistance to the initial crack formation but E rapidly decreased as the number of applied cycles increased.

The influence of t-ZrO_2 content was difficult to correlate with the observed drop in E after thermal cycles. Although the t-ZrO_2 content was scarce, AZ and MZz materials which had

the higher tetragonal phase content showed the best thermal shock resistance.

References

[1] P. Descamps, S. Sakaguchi, M. Poorteman, F. Cambier, J. Am. Ceram. Soc. 10 (1991) 2476–2481.
[2] N. Claussen, J. Jahn, J. Am. Ceram. Soc. (1980) 228–229.
[3] K. Das, S.K. Das, B. Mukherjee, G. Banerjee, Ceram. Int. 27 (2001) 833–837.
[4] L.B. Garrido, E.F. Aglietti, Ceram. Int. 5 (2001) 491–499.
[5] F. Temoche, L.B. Garrido, E.F. Aglietti, Ceram. Int. 31 (2005) 917–922.
[6] C. Aksel, Ceram. Int. 29 (2003) 311–316.
[7] C. Aksel, F. Komicezny, Glass Int. 1 (2001) 16–18.
[8] K. Das, S.K. Das, B. Mukherjee, G. Barnerjee, Interceram 5 (1998) 304–313.
[9] C. Aksel, Mater. Lett. 57 (2002) 992–997.
[10] C. Aksel, Ceram. Int. 29 (3) (2003) 305–309.
[11] S. Maitra, A. Rahaman, A. Sarkar, A. Tarafdar, Ceram. Int. 32 (2) (2006) 201–206.
[12] B.A. Boley, J.H. Weiner, Theory of Thermal Stresses, John Wiley & Sons, Inc., New York, 1960.
[13] D.P.H. Hasselman, J. Am. Ceram. Soc. 46 (1963) 535–540.
[14] D.P.H. Hasselman, J. Am. Ceram. Soc. 52 (1969) 600–604.
[15] M. Hamidouche, N. Bouaouadja, H. Osmani, R. Torrecillas, G. Fantochi, J. Eur. Ceram. Soc. 16 (1996) 441–445.
[16] ASTM standard C1525-04, Standard Test Method for Determination of Thermal Shock Resistance for Advanced Ceramics by Water Quenching, American Society for Testing and Materials, ASTM International, West Conshohoken, 2004.
[17] ASTM standard C1711-05.
[18] R.C. Garvie, P.S. Nicholson, J. Am. Ceram. Soc. 55 (1972) 303.
[19] W. Kingery, J. Am. Ceram. Soc. 38 (1955) 3–15.
[20] C. Baudin, Anales de mecánica de Fractura 7 (1990) 94–99.
[21] S. Lathabai, D.G. Hay, F. Wagner, N. Claussen, J. Am. Ceram. Soc. 79 (1996) 248.
[22] J. Luo, R. Stevens, Ceram. Int. 25 (1999) 281–286.